

# Energy & Environmental Science

Accepted Manuscript



This is an *Accepted Manuscript*, which has been through the Royal Society of Chemistry peer review process and has been accepted for publication.

*Accepted Manuscripts* are published online shortly after acceptance, before technical editing, formatting and proof reading. Using this free service, authors can make their results available to the community, in citable form, before we publish the edited article. We will replace this *Accepted Manuscript* with the edited and formatted *Advance Article* as soon as it is available.

You can find more information about *Accepted Manuscripts* in the [Information for Authors](#).

Please note that technical editing may introduce minor changes to the text and/or graphics, which may alter content. The journal's standard [Terms & Conditions](#) and the [Ethical guidelines](#) still apply. In no event shall the Royal Society of Chemistry be held responsible for any errors or omissions in this *Accepted Manuscript* or any consequences arising from the use of any information it contains.

Cite this: DOI: 10.1039/c0xx00000x

www.rsc.org/xxxxxx

FULL PAPER

## Enhanced thermal conductivity of phase change materials with ultrathin-graphite foams for thermal energy storage

Hengxing Ji,<sup>†</sup> Daniel P. Sellan,<sup>†</sup> Michael T. Pettes, Xianghua Kong, Junyi Ji, Li Shi\* & Rodney S. Ruoff\*<sup>5</sup> <sup>†</sup>These authors contributed equally to this work*Department of Mechanical Engineering and Materials Science and Engineering Program, The University of Texas at Austin, 1 University Station C2200, Austin, Texas 78712, United States.*

Received (in XXX, XXX) Xth XXXXXXXXX 20XX, Accepted Xth XXXXXXXXX 20XX

<sup>10</sup> DOI: 10.1039/b000000x

For thermophysical energy storage with phase change materials (PCMs), the power capacity is often limited by the low PCM thermal conductivity ( $\kappa_{\text{PCM}}$ ). Though dispersing high-thermal conductivity nanotubes and graphene flakes increases  $\kappa_{\text{PCM}}$ , the enhancement is limited by interface thermal resistance between the nanofillers, among other factors such as detrimental surface scattering of phonons. Here, we demonstrate that embedding continuous ultrathin-graphite foams (UGFs) with volume fractions as low as 0.8–1.2 vol.% in a PCM can increase  $\kappa_{\text{PCM}}$  by up to 18 times, with negligible change in the PCM melting temperature or mass specific heat of fusion. The composites increase in  $\kappa_{\text{PCM}}$ , thermal cycling stability, and applicability to a diverse range of PCMs suggests that UGF composites are a promising route to achieving the high power capacity targets of a number of thermal storage applications, including building and vehicle heating and cooling, solar thermal harvesting, and thermal management of electrochemical energy storage and electronics devices.

### Broader context

It has been envisioned that high-performance thermal energy storage technologies will play a broad and critical role in sustainable use of energy in heating and cooling applications, including building and vehicles heating and cooling, solar energy harvesting, and thermal management of electrochemical energy storage and electronic devices. Thermophysical energy storage based on phase change materials (PCMs) is one of the technologies being actively pursued. One major barrier that is currently preventing the broad adoption of many PCM-based technologies, however, is the very low thermal conductivity of available PCMs, which significantly limits the power capacity. Increasing the PCM thermal conductivity without affecting other performance criteria such as energy density or thermal cycling stability has been the focus of much research in recent decades, but only incremental performance advancements have been realized. In this work, we demonstrate significant thermal conductivity enhancement of PCMs with negligible change to other thermophysical properties by using continuous ultrathin-graphite foams (UGFs) to fabricate UGF-PCM composites. These findings represent an important step toward high-performance thermal energy storage technologies.

### 1 Introduction

<sup>20</sup> Thermal energy storage technologies have received renewed emphasis because of their critical role in a sustainable energy infrastructure. Both thermophysical and thermochemical storage methods are under active investigations.<sup>1</sup> Among the thermophysical storage approaches, phase change materials (PCMs) can be used to absorb and release thermal energy at a constant temperature during a phase transition, such as melting or solidification.<sup>1–4</sup> The thermal performance of PCMs is characterized by the melting temperature ( $T_m$ ), the energy density that is determined by the specific heat of fusion ( $\Delta H_{\text{fus}}$ ), and the thermal conductivity ( $\kappa_{\text{PCM}}$ ). System operating temperatures

dictate the  $T_m$  range. Novel PCMs with an appropriate  $T_m$  and high  $\Delta H_{\text{fus}}$  are needed to meet the energy density requirements for a broad adoption of PCM-based thermophysical storage technologies. Moreover, a large power capacity is needed to ensure sufficiently fast charging and discharging processes.

<sup>35</sup> The heat transfer rate that governs the power capacity is dominated by  $\kappa_{\text{PCM}}$ . PCMs, however, typically have low thermal conductivity in the range between 0.1–1 W m<sup>-1</sup> K<sup>-1</sup>, which is inadequate for meeting most power capacity targets unless bulky heat transfer devices are added with the consequence of reducing the system energy density.<sup>4</sup> Although high-thermal conductivity fillers can enhance the PCM thermal conductivity, the amount of fillers needs to be minimized so as to preserve a high energy

density. Continuous fillers such as copper-, aluminum-, nickel-, and carbon-foams have been shown to increase  $\kappa_{\text{PCM}}$ .<sup>5-10</sup> However, the improvements are limited by the solid thermal conductivity of the foam struts. Dispersed fillers with high thermal conductivity,<sup>11</sup> such as carbon fibers,<sup>12,13</sup> carbon nanotubes (CNTs),<sup>14,15</sup> graphite<sup>16,17</sup> and graphene flakes,<sup>18,19</sup> have also been used to increase  $\kappa_{\text{PCM}}$ . Despite the record-high thermal conductivity reported for suspended and clean CNTs and graphene,<sup>20-22</sup> only modest increases in  $\kappa_{\text{PCM}}$  have been observed in composites employing these fillers unless a high volume loading is used, which significantly reduces the energy density. For example, increasing  $\kappa_{\text{PCM}}$  by 11 times requires filling wax with over 4 vol.% graphite nanoplates,<sup>16</sup> while filling wax with 10 vol.% CNTs yields only 6 times improvement in the effective thermal conductivity.<sup>14</sup> Dispersed fillers can also be unstable during phase change. A recent study on graphite flake-hexadecane composites showed that the composite thermal conductivity can be changed by up to 3.2 times and electrical conductivity up to 2 orders of magnitude by varying the contact resistance between the dispersed graphite flakes during solid-liquid phase transition.<sup>23</sup> Although this effect can provide a means to tune the conductivity of composites and open up novel applications, the reduced thermal conductivity in the liquid state can decrease the heat transfer rate in PCM nanocomposites for the thermal storage application considered in this work.

Here we report an experimental investigation to show that ultrathin-graphite foam (UGF) with a low density of 1.2 vol.% can be used to increase  $\kappa_{\text{PCM}}$  by up to 18 times. The UGF struts retain the high basal-plane solid thermal conductivity of thin graphite,<sup>24</sup> while overcoming the thermal interface resistance issue found in van der Waals-bonded graphene and CNT networks. Because the UGFs are continuous, a rule of mixtures calculation is sufficient to explain the thermal conductivity enhancement in the UGF-PCM composites. The thermal conductivity enhancement is found to increase the rate of PCM melting even in an experiment setup with considerable parasitic loss. The electrical resistance of the UGF-PCM composites changed less than 2% over 100 solid-liquid phase transition cycles, indicating mechanical stability during thermal cycling. The mass specific heat of fusion and  $T_m$  of the PCM remain essentially unchanged after UGF loading, which overcomes a problem found in some PCM composites where the dispersed nanofillers results in considerable reduction of the heat of fusion.<sup>12,16,18,19</sup>

## 2 Results

### 2.1 Synthesis of UGFs and UGF-PCM composites

The UGF is grown on a nickel foam template (Fig. 1a, 1b and Video S1a) by chemical vapor deposition (CVD).<sup>25,26</sup> The nickel template is then removed by wet chemical etching, leaving only ultrathin-graphite struts connected in continuous foam architecture. The ultrathin-graphite struts are hollow, have an approximately triangular cross section, and are made of high-quality graphitic carbon with basal-plane parallel to the strut wall surface (Fig. 1c and Fig. S1). Because the as-grown UGFs are hydrophobic, they can be readily filled with hydrophobic paraffin wax, a common PCM, by immersing the foam in hot liquid wax (Fig. 1d, 1f, 1h and Video S1b). This process yields UGF-PCM

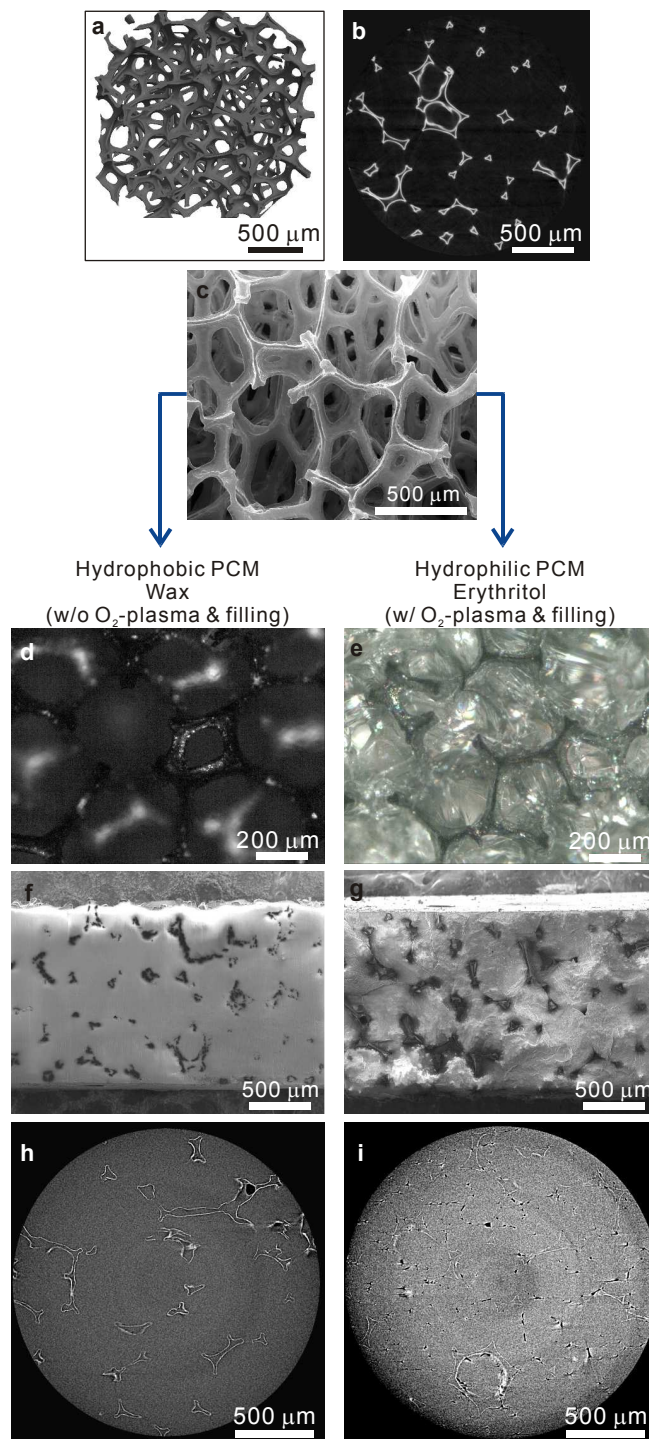


**Fig. 1** (a) Reconstructed three-dimensional micro-computed tomography (CT) scan and (b) single micro-CT scan slice of the nickel foam template. (c) Scanning electron micrograph (SEM) of UGF after growth and nickel removal and before PCM filling. Differential interference contrast images of (d) UGF-wax composite and (e) UGF-erythritol composite. Cross-sectional SEMs of (f) UGF-wax composite and (g) UGF-erythritol composite. Micro-CT scan slices of (h) UGF-wax composite and (i) UGF-erythritol composite.

composites with high PCM filling fraction,  $\phi_{\text{PCM}} = 95.8 \pm 0.4$  vol.% or  $97.3 \pm 0.1$  wt.%. To obtain the PCM volume fraction ( $\phi_{\text{PCM}}$ ), the weight of the bare UGF ( $w_{\text{UGF}}$ ) and UGF-PCM composite ( $w_{\text{Comp}}$ ) was measured using a mass balance

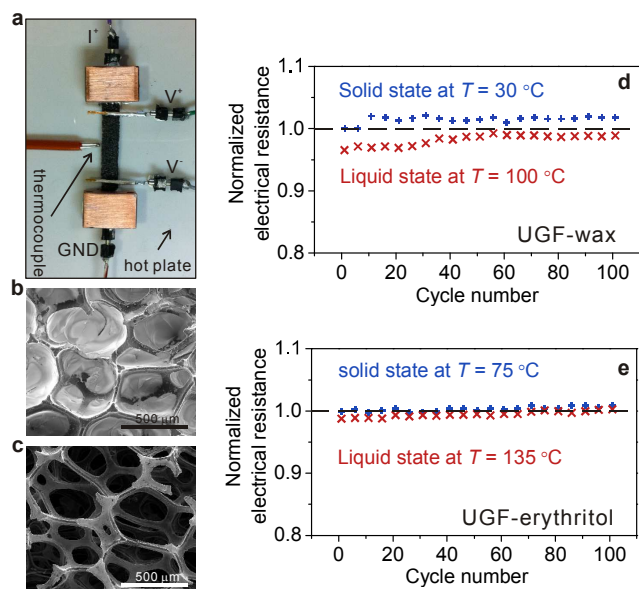


**Fig. 2** (a) Photograph of the four-probe electrical measurement setup for a UGF-composite sample placed on a hot plate. Scanning electron micrographs of UGF-erythritol composite (b) after 100 heating and cooling cycles and (c) after subsequent removal of erythritol by washing with de-ionized water. The UGF struts remained unchanged after 100 cycles of liquid-solid phase change of PCM. Electrical resistance measured in the solid state (blue) and liquid state (red) normalized by the resistance of the solid state measured during the first heating cycle of (d) UGF-wax composite with  $\phi_{\text{foam}} = 0.84 \pm 0.02\%$  and  $\phi_{\text{PCM}} = 98 \pm 0.4\%$  and (e) UGF-erythritol composite with  $\phi_{\text{foam}} = 0.84 \pm 0.02\%$  and  $\phi_{\text{PCM}} = 85 \pm 0.4\%$  during 100 heating/cooling cycles.

(XP105DR, Mettler Toledo). The difference gives the net weight of the PCM. The volume of the UGF-PCM composite ( $V_{\text{Comp}}$ ) was then measured using a vernier caliper. The PCM volume fraction is then calculated as  $(w_{\text{Comp}} - w_{\text{UGF}}) / (\rho_{\text{PCM}} V_{\text{Comp}})$ , where  $\rho_{\text{PCM}}$  is the density of the pure PCM. In comparison to the wax composites, filling the UGFs with hydrophilic food-grade erythritol PCM required that the UGF first be functionalized with C-O groups via an oxygen plasma treatment<sup>27</sup> to make the UGF surface hydrophilic (Fig. S2a). The UGF electrical resistivity remained unchanged after surface functionalization (Fig. S2b), suggesting that the brief oxygen plasma exposure affected only the surface without damaging the UGF structure. After surface functionalization, the UGF was immersed in hot liquid erythritol (Fig. 1e, 1g, 1i). The electrical resistivity of the UGF sample remained unchanged after filling with erythritol (Fig. S2b). A scanning electron micrograph (Fig. 1g) and micro-CT scan slices (Fig. 1i and Video S1c) of the UGF-erythritol composites reveal that even the hollow interior of the UGF struts is filled with PCM using this process. Nevertheless, the filling fractions of the UGF-erythritol composites,  $\phi_{\text{PCM}} = 85.9 \pm 1.6 \text{ vol.}\%$  or  $98.2 \pm 0.1 \text{ wt.}\%$ , were consistently less than those of the UGF-wax composites. Micro-CT scan slices show that voids are distributed throughout the entire UGF-erythritol composite (Fig. 1i), while voids are intermittent in UGF-wax composites (Fig. 1h). It is possible that voids in the UGF-erythritol composite form during solidification because the UGF-struts impede the natural formation of large erythritol crystallites, which based on our experiments are on the order of several millimeters in pure erythritol (see Fig. S3). This issue is not observed in the UGF-

wax composites. In comparison, a 10% decrease in density was reported in aligned CNT-array polymer composites with 0.4 vol.% filler due to the presence of voids in the composites.<sup>15</sup> Similarly, voids were responsible for 9–13% decrease in density when high-density carbon foams ( $\phi_{\text{foam}} = 19\text{--}46 \text{ vol.}\%$ )<sup>6</sup> as well as low-density copper and nickel foams ( $\phi_{\text{foam}} = 3 \text{ vol.}\%$ )<sup>7</sup> were filled with wax.

## 2.2 Stability test of UGF-PCM composites

One requirement for a PCM composite is that it must be stable after multiple melting and solidification cycles. We evaluated the thermal cycling stability of the UGF-PCM composite by measuring the sample electrical resistance during multiple melting and solidification cycles. For the electrical measurements, copper electrodes were attached using silver epoxy to the UGF before it was filled with PCM to ensure good electrical contact over the melting and solidification cycles (Fig. 2a). These electrodes were used to measure the four-probe electrical resistance of the sample. During melting of the PCM in the composite samples, the liquid PCM remained in the UGF scaffold because of surface tension, so that there was negligible mass loss during electrical measurements over 100 melting and solidification cycles. In thermal storage devices, PCM is usually enclosed in a container to prevent leakage of liquid PCM. Figure 2d and Fig. 2e present the electrical resistance of the UGF-wax composite and the UGF-erythritol composite, respectively, in the solid state and liquid state over 100 melting and solidification cycles. The difference in UGF-PCM composite electrical resistance measured in the two states is attributed to the temperature dependence of the UGF electrical resistivity (Fig. S4). The change in the electrical resistance after 100 melting and solidification cycles is less than 2% for both UGF-wax and UGF-erythritol composites, indicating that the UGFs buried in PCMs are mechanically stable during cycling. SEM images of the UGF after removal of erythritol also indicate that the UGF structure did not change after the 100 cycles (Figs. 2b and 2c). In comparison, filler settling has been reported in composites with dispersed fillers,<sup>12,15,17,18</sup> which results in a composite thermal conductivity reduction upon cycling. Because the UGF structure is stable upon thermal cycling, this effect is expected to be absent in the UGF-PCM composites investigated here.

## 2.3 Heat of fusion of UGF-PCM composites

The energy density of the UGF-PCM composites is dominated by  $\Delta H_{\text{fus}}$ , which was measured using a Netzsch DSC-404 F1 Pegasus differential scanning calorimetry (DSC). The DSC measurement results are presented in Fig. 3 and Table S1. Several studies have shown that adding fillers to a PCM can change  $\Delta H_{\text{fus}}$  because there is less PCM per unit volume or per unit mass and the dispersed fillers can interrupt the local bonding environment of the PCM molecules.<sup>12,16-19</sup> While some studies report decreased  $\Delta H_{\text{fus}}$  after filler loading, other studies report negligible  $\Delta H_{\text{fus}}$  change. For instance, Fan et al.<sup>19</sup> reported that dispersing carbon nanotubes, carbon nanofibers, or graphene nanoplatelets in paraffin wax systematically decreased the mass specific heat of fusion for all filler types, by up to 10% with 1 wt% filler loading. In comparison, Kim et al.<sup>17</sup> report no significant change in heat of fusion when up to 5 wt.% of exfoliated graphite nanoplatelets

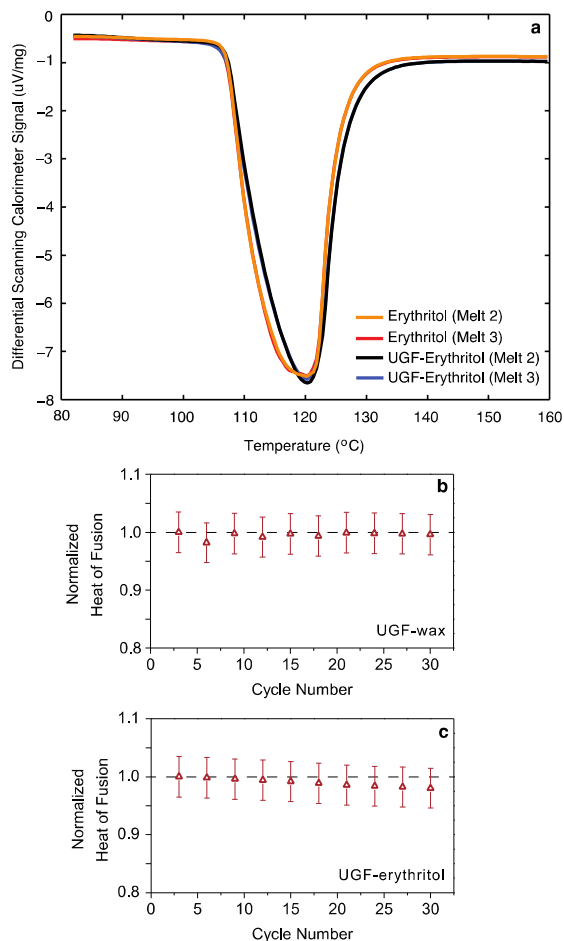


**Fig. 3** (a) Differential scanning calorimeter (DSC) plot of melting of pure erythritol and UGF-erythritol composite. The results shown in this plot are representative of the DSC data obtained for all samples. The obtained mass specific heat of fusion normalized by the first heating cycle of (c) un-annealed UGF-wax composite and (d) un-annealed UGF-erythritol composite after 30 heating/cooling cycles.

were dispersed in paraffin wax. In this study, negligible change in the mass specific heat of fusion has been found for the UGF-PCM composites compared to the pure PCMs values,  $\Delta H_{\text{fus}} = 339 \pm 10 \text{ J g}^{-1}$  for erythritol and  $\Delta H_{\text{fus}} = 189.3 \pm 5.7 \text{ J g}^{-1}$  for wax. This finding is attributed to the relatively large,  $\sim 500 \mu\text{m}$  diameter pore size of the UGF, and consequently a relatively small filler-PCM interface area of about  $\sim 0.6 \text{ m}^2 \text{ g}^{-1}$ ,<sup>25</sup> compared to the  $\sim 30 \text{ m}^2 \text{ g}^{-1}$  value found for exfoliated graphite nanoplatelets<sup>17</sup> and  $\sim 300 \text{ m}^2 \text{ g}^{-1}$  for CNT fillers.<sup>14</sup> As such, the melting and solidification processes of the pure PCM inside the large pores are not affected by the UGF. For this reason, negligible change in the PCM melting temperature was also found for the UGF-PCM composites compared to the pure PCM values,  $T_m = 120.2^\circ\text{C}$  for erythritol and  $T_m = 58.9^\circ\text{C}$  for wax, as illustrated by the DSC plot in Fig. 3a for the UGF-erythritol composite. In addition, only a less than 2% reduction in heat of fusion was observed over the 30 solid-liquid phase transition cycles for the UGF-PCM composites, as shown in Fig. 3b for the UGF-wax composite and Fig. 3c for the UGF-erythritol composite. The small reduction in the heat of fusion for the UGF-erythritol sample is attributed to PCM evaporation and mass loss during the 30-cycle DSC measurement. The evaporation occurs

because the measurement was performed in an environment of constant flow of dry helium gas. Such losses are not present in an actual thermal storage device where the PCM is enclosed inside a container.

#### 2.4 Thermal conductivity of UGFs and UGF-PCM composites

Because of the open-cell structure and low density of the unfilled UGFs, established thermal conductivity measurement techniques<sup>29</sup> such as the steady-state reference method and transient laser flash technique cannot be applied to these samples.<sup>30</sup> To address this challenge, a self-electrical-heating method has been demonstrated in a previous work to measure the thermal conductivity of unfilled UGFs ( $\kappa_{\text{foam}}$ ).<sup>24</sup> During self-electrical-heating of the UGF sample, the change in electrical resistance of the UGF was measured and used to determine the average temperature rise. The thermal conductivity of the UGF is then obtained by using the applied Joule heating power and corresponding average temperature rise as inputs to a combined heat conduction and radiation loss model, as discussed in the Supplementary Information.

In addition, although the laser flash method has been successfully used in this work to measure the thermal conductivity of the pure PCM, we found that the transient thermal response data obtained by this technique on the UGF-PCM composites show poor agreement with the several one-dimensional transient heat conduction models commonly used to interpret the laser flash measurement results. In the UGF-PCM composites, we expect that the heat pulse travels more readily through the high thermal conductivity continuous UGF struts than the low thermal conductivity PCM, so that the established models for homogenous materials cannot accurately describe transient thermal transport in the UGF composites.

In this work, the steady state self-electrical-heating method has been employed for thermal conductivity measurements of both unfilled UGFs and filled UGF composites, whereas a steady state reference method has also been used to measure the thermal conductivity of a filled UGF composite sample and verify the self-heating measurement result. Using the self-electrical-heating method allowed us to compare the thermal conductivity of an unfilled UGF and a filled UGF-PCM composite for the same UGF sample, thus eliminating sample-to-sample variability.

In the steady-state measurement technique, an un-annealed UGF-erythritol composite sample ( $\square_{\text{foam}} = 1.23 \pm 0.02\%$ ,  $\phi_{\text{PCM}} = 84 \pm 0.4\%$ ) was connected with a constantan bar reference (see Fig. S6 in Supplementary Information for details). The assembly was sandwiched between a resistance heater and a copper heat sink to establish a linear temperature profile, which was measured using two differential Type-T thermocouples. Like the self-electrical-heating measurement, this measurement was performed in high vacuum ( $< 10^{-6}$  torr) to eliminate convective losses. With radiation loss from the circumference of the sample and reference accounted for, the steady-state reference method was found to yield  $\kappa_{\text{comp}} = 2.8 \pm 0.3 \text{ W m}^{-1} \text{ K}^{-1}$ .

The self-electrical-heating measurement results for unfilled UGFs are shown as open circles in Fig. 4a and Table S1. Although the volume fractions of  $\square_{\text{foam}} = 1.23, 0.88,$  and  $0.83 \text{ vol.}\%$  for the three UGFs evaluated here are similar to those of van der Waals-bonded single-walled carbon nanotube aerogels reported

recently,<sup>31</sup> the obtained  $\kappa_{\text{foam}}$  are two orders of magnitude larger than the  $0.025 \text{ W m}^{-1} \text{ K}^{-1}$  value reported for an aerogel with volume fraction  $\phi_{\text{aerogel}} = 0.61 \text{ vol.}\%$ . The UGF with  $\phi_{\text{foam}} = 1.23 \text{ vol.}\%$  was annealed at a temperature of  $3000 \text{ }^\circ\text{C}$  for one hour in an argon environment, while the other two foams were not annealed. The solid strut thermal conductivity of the annealed UGF,  $\kappa_{\text{strut}} = 840 \text{ W m}^{-1} \text{ K}^{-1}$ , which was calculated using the metal foam theory<sup>32</sup>  $\kappa_{\text{strut}} = (3/\phi_{\text{foam}})\kappa_{\text{foam}}$ , is a factor of 1.6 larger than the average value of the foams that were not annealed,  $\sim 520 \text{ W m}^{-1} \text{ K}^{-1}$ , over two times larger than copper,  $\kappa_{\text{copper}} \sim 400 \text{ W m}^{-1} \text{ K}^{-1}$ , and approaching values reported for high-quality graphite.<sup>33</sup>

Based on the average thermal conductivity for the un-annealed UGF struts found from the self-electrical-heating method,  $\kappa_{\text{strut}} \sim 520 \text{ W m}^{-1} \text{ K}^{-1}$ , and the solid volume fraction of the UGF sample measured using the steady-state technique ( $\phi_{\text{foam}} = 1.23 \pm 0.02\%$ ), the UGF thermal conductivity is predicted by the metal foam theory to be  $\kappa_{\text{foam}} = 2.13 \text{ W m}^{-1} \text{ K}^{-1}$ . In addition, the thermal conductivities of the paraffin wax and the food-grade erythritol measured by the laser flash method are  $\kappa_{\text{PCM}} = 0.20 \pm 0.02 \text{ W m}^{-1} \text{ K}^{-1}$  and  $\kappa_{\text{PCM}} = 0.81 \pm 0.09 \text{ W m}^{-1} \text{ K}^{-1}$ , respectively. The UGF-erythritol composite thermal conductivity result obtained by the steady-state method agrees well with a rule of mixtures calculation,  $\kappa_{\text{comp}} = \kappa_{\text{foam}} + \phi_{\text{PCM}} \kappa_{\text{PCM}}$ , without needing to account for interface thermal conductance. There are two reasons for this agreement. First, the foam and the PCM are each continuous in the composite. Second, because the UGF strut wall thicknesses are on the order of hundreds-of-nanometers to a few microns, their thermal conductivity is insensitive to phonon scattering at the graphite strut/PCM interface. In comparison, such interface scattering has been found to considerably reduce the basal-plane thermal conductivity of few-layer graphene and few-layer hexagonal boron nitride.<sup>34-36</sup>

Upon completion of the self-electrical-heating measurements of unfilled UGF samples, two of the measured foam samples were filled with paraffin wax. The remaining foam sample was filled with food-grade erythritol. Because the three foam samples were suspended on the sample stage for thermal conductivity measurements, they could not be filled using the immersion process discussed above, and instead were filled by dropping hot liquid PCM onto the suspended foam sample, resulting in lower PCM filling fractions between 77–88 vol.% (Table S1). The thermal conductivity results of the UGF-PCM composites,  $\kappa_{\text{comp}}$ , measured using the same self-electrical-heating method are shown as filled circles in Fig. 4a and appear in Table S1. Because the PCM is electrically insulating and has a relatively low thermal conductivity, it is a concern whether an appreciable local temperature difference is present between the electrically heated UGF and the surrounding PCM, which would result in an underestimation of the UGF-PCM composite thermal conductivity in the self-heating measurement. To evaluate this effect, we compare the UGF-PCM composite thermal conductivity measured from the rule of mixture calculation. Similar to that found for the steady-state method, the  $\kappa_{\text{comp}}$  values obtained from the self heating method is in good agreement with the rule of mixture calculation based on the measured UGF thermal conductivity from the self-heating method, PCM thermal conductivity from the laser flash method, and the measured volume fractions. This finding suggests that the steady state

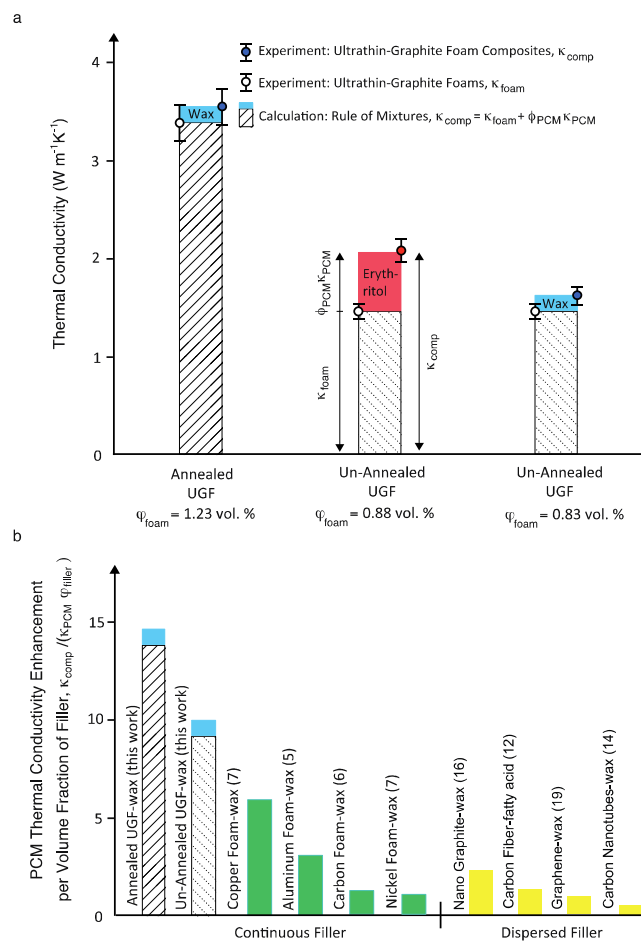


**Fig. 4** (a) Measured thermal conductivity of unfilled UGFs,  $\kappa_{\text{foam}}$ , (open circles) and UGF-PCM composites,  $\kappa_{\text{comp}}$ , (filled circles) at near room temperature. Shown for comparison are results from rule of mixtures calculations. (b) Comparison of PCM thermal conductivity enhancement per volume fraction of filler for the UGF-wax composites in this work and different fillers reported in literature. All PCMs in (b) have thermal conductivity in the range of  $\kappa_{\text{PCM}} = 0.17\text{--}0.31 \text{ W m}^{-1} \text{ K}^{-1}$ .

reference method and the self-heating technique yield consistent UGF-PCM thermal conductivity values.

### 3 Discussion

Even at the very low loading fractions, the UGF-PCM composite thermal conductivities represent an improvement over the base PCMs by up to a factor of 18. To put these results into perspective, in Fig. 4b we compare the PCM thermal conductivity enhancement per volume fraction of filler for the UGF-wax composites presented here and other continuous filler composites (aluminium foam,<sup>5</sup> carbon foam,<sup>6</sup> copper foam,<sup>7</sup> and nickel foam<sup>7</sup>) and discrete filler composites (carbon fiber<sup>12</sup>, carbon nanotube<sup>14</sup>, nano-graphite<sup>16</sup> and graphene<sup>18</sup>) reported in literature. This performance metric is useful for thermophysical energy storage applications because it reflects the need to minimize the filler loading used to enhance thermal conductivity so as to preserve a high energy density. Because the UGF consists of high-quality graphite struts, the strut solid thermal conductivity is higher than that found in metal and other carbon foams, resulting in greater performance. Because carbon has a low atomic weight compared to aluminium and copper, the UGF is expected to out

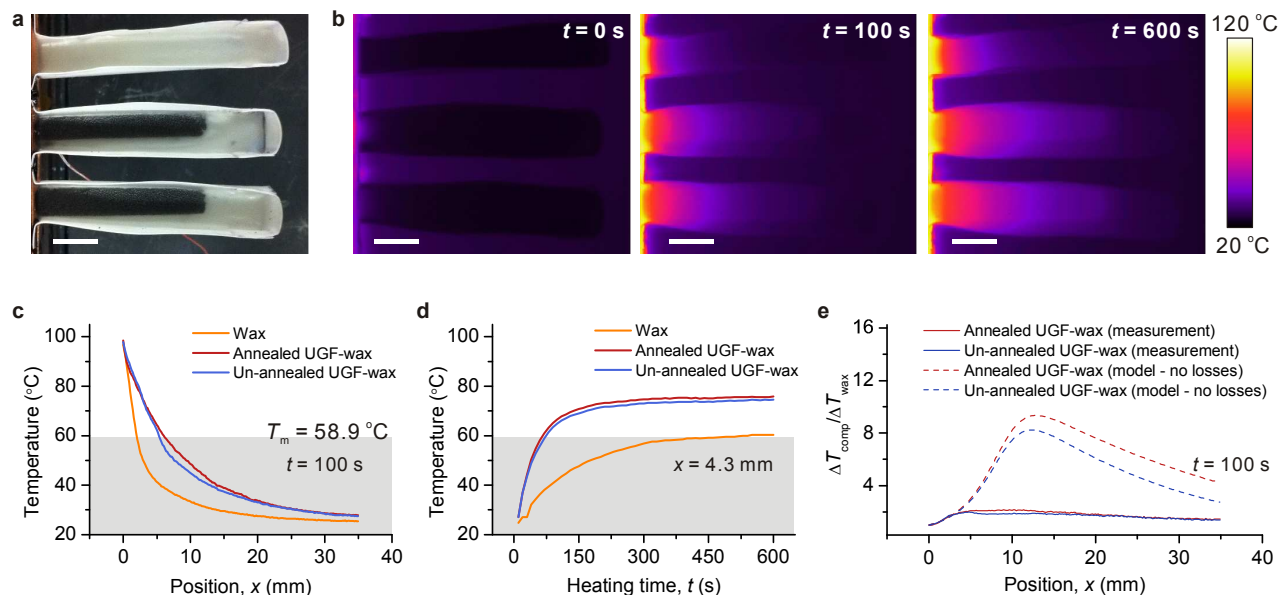


**Fig. 5** (a) Photograph of three samples loaded in Teflon holders for transient melting study. The top sample is pure paraffin wax, while the bottom two samples are un-annealed UGF-wax ( $\phi_{\text{foam}} = 1.42 \pm 0.04$  vol.%) and annealed UGF-wax ( $\phi_{\text{foam}} = 1.37 \pm 0.03$  vol.%) composites. (b) The temperature profile evolutions in time of three samples shown in (a) were captured using a calibrated infrared camera and are presented at  $t = 0, 100,$  and  $600$  s. (c) A temperature profile along the middle of each sample after 100 seconds of heating. (d) Temperature as a function of time at the position  $x = 4.3$  mm. (e) Measured temperature enhancement,  $\Delta T_{\text{comp}}/\Delta T_{\text{wax}}$ , as a function of position after 100 seconds of heating for both the annealed and un-annealed UGF-wax composites. For comparison, theoretical predictions for the case where there is no parasitic heat loss by convection and radiation is also provided in (e). All scale bars indicate 10 mm.

perform the metal foams to an even greater extent than in Fig. 4b when compared on a weight basis. Conversely, the thermal interface resistance present between discrete fillers results in a much lower composite thermal conductivity than the continuous UGF-PCM composites at the same loading. For example, around 1.5 times enhancement in thermal conductivity was reported for a wax sample loaded with 1.3 vol% graphene nanoplatelets.<sup>19</sup> This value is much lower than the 18 times increase in  $\kappa_{\text{PCM}}$  observed in the annealed UGF-wax composites at a similar filler loading fraction.

To demonstrate the effect on thermal performance of  $\kappa_{\text{PCM}}$  using UGFs, results from a transient melting study are presented in Fig. 5. The temperature profile evolution in time of three samples was captured using a calibrated infrared camera (see Figs. S7 and S8 in Supplementary Information for details) as the samples were heated from one side (Fig. 5a and 5b). As shown in Figs. 5c and 5d, the temperature as a function of position and heating time data indicate that heat penetrated further and temperature increased quicker for the two UGF-wax composite samples than the pure wax sample, resulting in a faster PCM melting rate. The temperature enhancement,  $\Delta T_{\text{comp}}/\Delta T_{\text{wax}}$ , at  $t = 100$  seconds is presented as a function of position in Fig. 5e. Because the measurement was performed in ambient conditions, radiative and convective losses from the sample become large compared to heat conduction through the sample for regions more than 5 mm away from the heat source. Such losses are not present in an actual thermal storage device where the PCM is thermally insulated inside a container. Using a 1D phase change model based on Neumann's solution for melting of a semi-infinite region to model the transient melt process,<sup>37</sup> elimination of the losses can result in even larger enhancement for regions away from the heat source, as shown in Fig. 5e.

## 4 Conclusions

These experimental results demonstrate that loading a paraffin wax PCM with annealed UGF can significantly increase  $\kappa_{\text{PCM}}$  by as much as a factor of 18 with cycling stability and negligible change in the PCM melting temperature or mass specific heat of fusion. Even larger thermal performance enhancement may be possible by optimizing the UGF geometry, such as reducing the pore size of the foam. Such enhancement can result in an increase of the power capacity of PCM-based thermophysical storage devices to meet the requirements of a number of heating and cooling applications. The thermal conductivity of the UGF-PCM composites is well described by a rule of mixtures calculation, which simplifies the design process of thermophysical storage devices using the UGF-PCM composites. In addition, the sacrificial nickel used to grow the UGF can be recycled,<sup>38</sup> and the UGF sample size is readily scalable (Fig. S9). Moreover, recent works have shown that it is possible to grow carbon nanotubes that anchor to the foam struts and extend into the foam pore,<sup>39</sup> which presents another exciting direction to further increase the heat transfer rate when such hybrid foams are used in PCM composites.

## Acknowledgements

The authors thank Wei Shih at Allcomp, Inc. for post-synthesis annealing of the UGF samples, Prabhakar Marepalli and Jessie Maisano for acquiring and processing all micro-CT scans, Alex da Silva, Evan Fleming, and Shoayi Wen for use of the infrared camera and helpful discussions, and Alan J.H. McGaughey for

helpful discussions. This work is supported by US Department of Energy ARPA-E HEATS program, Award # DE-AR0000178.

## Notes and references

†These authors contributed equally to this work

<sup>5</sup> Department of Mechanical Engineering and Materials Science and Engineering Program, The University of Texas at Austin, Austin, Texas 78712, United States.

<sup>10</sup> \*E-mail: r.ruoff@mail.utexas.edu, lishi@mail.utexas.edu

Electronic Supplementary Information (ESI) available: [details of any supplementary information available should be included here]. See DOI: 10.1039/b000000x/

- <sup>1</sup> I. Gur, K. Sawyer and R. Prasher, *Science*, 2012, **335**, 1454.
- <sup>2</sup> Z. H. Rao and S. F. Wang, *Renew. Sust. Energ. Rev.*, 2011, **15**, 4554.
- <sup>3</sup> S. Wang and M. Baldea, *Ind. Eng. Chem. Res.*, 2013, **52**, 3247.
- <sup>4</sup> H. Mehling and L. F. Cabeza, *Heat and cold storage with PCM-An up to date introduction into basics and applications*, Springer, Berlin 2008.
- <sup>5</sup> K. Lafdi, O. Mesalhy and S. Shaikh, *J. Appl. Phys.*, 2007, **102**, 083549.
- <sup>6</sup> O. Mesalhy, K. Lafdi and A. Elgafy, *Carbon*, 2006, **44**, 2080.
- <sup>7</sup> X. Xiao, P. Zhang and M. Li, *Applied Energy*, 2013, **112**, 1357
- <sup>8</sup> W. Q. Li, Z. G. Qu, Y. L. He and W. Q. Tao, *Appl. Therm. Eng.*, 2012, **37**, 1.
- <sup>9</sup> M. Zhou, T. Lin, F. Huang, Y. Zhong, Z. Wang, Y. Tang, H. Bi, D. Wan and J. Lin, *Adv. Funct. Mater.*, 2012, **23**, 2263.
- <sup>10</sup> K. Boomsma and D. Poulikakos, *Int. J. Heat Mass Tran.*, 2001, **44**, 827.
- <sup>11</sup> A. A. Balandin, S. Ghosh, W. Bao, I. Calizo, D. Teweldebrhan, F. Miao and C. N. Lau, *Nano Lett.*, 2008, **8**, 902.
- <sup>12</sup> J. Wang, H. Xie, Z. Xin, Y. Li and C. Yin, *J. Appl. Phys.*, 2011, **110**, 094302.
- <sup>13</sup> A. Elgafy and K. Lafdi, *Carbon*, 2005, **43**, 3067.
- <sup>14</sup> L. Chen, R. Zou, W. Xia, Z. Liu, Y. Shang, J. Zhu, Y. Wang, J. Lin, D. Xia, and A. Cao and ACS Nano, 2012, **6**, 10884.
- <sup>15</sup> H. Huang, C. H. Liu, Y. Wu and S. S. Fan, *Adv. Mater.*, 2005, **17**, 1652.
- <sup>16</sup> J.-N. Shi, M.-D. Ger, Y.-M. Liu, Y.-C. Fan, N.-T. Wen, C.-K. Lin and N.-W. Pu, *Carbon*, 2013, **51**, 365.
- <sup>17</sup> S. Kim and L. T. Drzal, *Sol. Energy Mater. Sol. Cells*, 2009, **93**, 136.
- <sup>18</sup> F. Yavari, H. R. Fard, K. Pashayi, M. A. Rafiee, A. Zamiri, Z. Yu, R. Ozisik, T. Borca-Tasciuc and N. Koratkar, *J. Phys. Chem. C*, 2011, **115**, 8753.
- <sup>19</sup> L.-W. Fan, X. Fang, X. Wanga, Y. Zeng, Y.-Q. Xiao, Z.-T. Yu, X. Xuc, Y.-C. Hua and K.-F. Cen, *Applied Energy*, 2013, **110**, 163.
- <sup>20</sup> A. A. Balandin, *Nature Mater.*, 2011, **10**, 569.
- <sup>21</sup> L. Shi, *Nanoscale Microsc. Therm.*, 2012, **16**, 79.
- <sup>22</sup> P. Kim, L. Shi, A. Majumdar and P. L. McEuen, *Phys. Rev. Lett.*, 2001, **87**, 215502.
- <sup>23</sup> R. Zheng, J. Gao, J. Wang and G. Chen, *Nature Commun.*, 2011, **2**, 289.
- <sup>24</sup> M. T. Pettes, H. Ji and R. S. Ruoff, L. Shi, *Nano Lett.*, 2012, **12**, 2959.
- <sup>25</sup> H. Ji, L. Zhang, M. T. Pettes, H. Li, S. Chen, L. Shi, R. Piner and R. S. Ruoff, *Nano Lett.*, 2012, **12**, 2446.
- <sup>26</sup> Z. Chen, W. Ren, L. Gao, B. Liu, S. Pei and H.-M. Cheng, *Nature Mater.*, 2011, **10**, 424.
- <sup>27</sup> U. Cvelbar, B. Markoli, I. Poberaj, A. Zalar, L. Kosec and S. Spaic, *Appl. Surf. Sci.*, 2006, **253**, 1861.
- <sup>28</sup> Y. Zhu, S. Murali, W. Cai, X. Li, J. W. Suk, J. R. Potts and R. S. Ruoff, *Adv. Mater.*, 2010, **22**, 3906.
- <sup>29</sup> C.L. Tien, A. Majumdar and F. F. M. Gerner, *Microscale Energy Transport*, Taylor & Francis, Washington, D.C., 1989.
- <sup>30</sup> We performed both the laser flash and steady-state measurements on unfilled UGF samples. During the laser flash method measurements (Netzsch LFA-457 micro flash, see Supplementary Information for details), almost all of the laser energy intended to heat the sample surface passed through the unfilled UGF samples because they have an open-cell structure and are over 98% void space, thus, rendering the measurement impossible for the as-grown unfilled UGF samples. For steady-state reference measurements on the unfilled UGF samples, we found the error associated with accurately measuring the temperature of the unfilled UGF struts was unsatisfactory. We therefore use the self-electrical-heating method to measure the thermal conductivity of the unfilled UGFs.
- <sup>31</sup> S. N. Schiffres, K. H. Kim, L. Hu, A. J. H. McGaughey, M. F. Islam and J. A. Malen, *Adv. Funct. Mater.*, 2012, **22**, 5251.
- <sup>32</sup> M. A. Schuetz and L. R. Glicksman, *J. Cell. Plast.*, 1984, **20**, 114.
- <sup>33</sup> Y.S. Touloukian, R.W. Powell, C.Y. Ho and P.G. Klemens, *Thermal conductivity—nonmetallic solids*, in: Y.S. Touloukian, C.Y. Ho (Eds.), *Thermophysical properties of Matter*, IFI/Plenum, NewYork, 1970.
- <sup>34</sup> J. H. Seol, I. Jo, A. L. Moore, L. Lindsay, Z. H. Aitken, M. T. Pettes, X. Li, Z. Yao, R. Huang, D. Broido, N. Mingo, R. S. Ruoff and L. Shi, *Science*, 2010, **328**, 213.
- <sup>35</sup> M. T. Pettes, I. Jo, Z. Yao and L. Shi, *Nano Lett.* 2011, **11**, 1195.
- <sup>36</sup> I. Jo, M. T. Pettes, J. Kim, K. Watanabe, T. Taniguchi, Z. Yao and L. Shi, *Nano Lett.*, 2013, **13**, 550.
- <sup>37</sup> L. M. Jiji, *Heat Conduction*, Begell House, New York 2003.
- <sup>38</sup> F. F. K. Crundwell, M. S. Moats, V. Ramachandran, T. G. Robinson and W. G. Davenport, *Extractive Metallurgy of Nickel, Cobalt and Platinum-Group Metals*, Elsevier Science & Technology Books, Oxford 2011.
- <sup>39</sup> Z. Yan, L. Ma, Y. Zhu, I. Lahiri, M. G. Hahm, Z. Liu, S. Yang, C. Xiang, W. Lu, Z. Peng, Z. Sun, C. Kittrell, J. Lou, W. Choi, P. M. Ajayan and J. M. Tour, *ACS Nano*, 2013, **7**, 58.